THE ASTROPHYSICAL JOURNAL, 488:397–408, 1997 October 10

ASCA X-RAY SPECTROSCOPY OF THE UNUSUAL B0 V STAR τ SCORPII

D. H. COHEN,[1,2] J. P. CASSINELLI,[1] AND W. L. WALDRON[3]

Received 1996 December 16; accepted 1997 May 27

ABSTRACT

We have obtained a high-quality *ASCA* spectrum of the MK standard B0 V star τ Sco in order to test the standard wind-shock picture of OB star X-ray production. The fluxes in three line complexes from ions indicative of hot plasma—Mg^{+10}, Si^{+12}, and S^{+14}—are measured, and we also present a global spectral fit using a fairly standard multitemperature, optically thin, collisional equilibrium model. We were able to achieve a statistically good fit, but only by using the MeKaL plasma emission code (Mewe, Kaastra, & Liedahl) and fixing the elemental abundances at the photospheric values as determined by optical spectroscopy. The parameters of the model are $T_1 = 7$ MK, $EM_1 = 3.5 \times 10^{54}$ cm^{-3}, $T_2 = 12$ MK, $EM_2 = 8.1 \times 10^{53}$ cm^{-3}, $T_3 > 27$ MK, $EM_3 > 3.0 \times 10^{53}$ cm^{-3}. The quantity of material with temperature in excess of 10^7 K on τ Sco is comparable to that with temperature in excess of 10^6 K on most other early B stars.

The data cannot be explained by the standard line-force instability wind-shock mechanism. However, more unusual shock mechanisms involving magnetically confined wind shocks or interactions between infalling matter and the ambient stellar wind cannot be ruled out. Alternately, a dynamo driven by differential rotation could be powering coronal plasma. If magnetic fields are involved in any way, then the star's extreme youth could play a role.

Subject headings: radiation mechanisms: nonthermal — stars: atmospheres — stars: early-type — stars: individual: τ Sco — X-rays: stars

1. INTRODUCTION

The *ASCA* Solid State Imaging Spectrometers (SIS0 and SIS1), with their moderate spectral resolution, have opened up new possibilities for diagnosing the properties of hot astrophysical plasmas, including those observed on OB stars. The resolution and hard-energy response of *ASCA* is especially useful for testing the limits of the commonly accepted picture of wind shocks in early-type stars. τ Sco is a well-studied and unusual B0 star with previous low-resolution X-ray observations that have been difficult to explain in terms of wind shocks. In this paper we will analyze *ASCA* SIS observations, including the fluxes of several strong X-ray emission line complexes, to see if other high-energy mechanisms must be invoked in at least this one early-type star.

Although OB stars have been known to be X-ray sources for almost 20 years, there is still no completely viable explanation for the origin of the X-rays. Coronal regions were proposed even before the actual discovery of hot star X-rays (Cassinelli & Olson 1979), but despite elaboration of a coronal/wind hybrid model (Waldron 1984), this picture has very little supporting evidence. Many different shock models have been proposed since then (Lucy & White 1980; Lucy 1982; Mullan 1984; Abbott & Friend 1989; MacFarlane & Cassinelli 1989; Bjorkman & Cassinelli 1993; Porter & Drew 1995). Most researchers now assume that wind shocks are the origin of the observed X-rays in most OB stars, and the mechanism that is most often invoked—because of its sound physical basis and the numerical explorations that have been performed—is the line-force instability mechanism.

Briefly, the line-force instability exists in supersonic line-driven outflows because of the asymmetric shadowing of the spectral line profiles of wind material by the slower moving upstream wind flow. Any positive velocity perturbation of a parcel of gas moves the parcel out of the Doppler shadow of the material behind it, increasing the line force and further increasing the parcel's velocity. Recently, detailed numerical simulations of stellar winds with the line-force instability, which include radiation losses in the energy equation but assume spherical symmetry, have been performed by Cooper (1994) and Feldmeier (1995). These simulations reveal a highly structured wind with many shocks beyond a few tenths of a stellar radius. These shocks are primarily reverse shocks, in which rarefied gas is accelerated into slower moving material, and therefore only a very small fraction of the wind material is heated to X-ray–emitting temperatures at any one time. This small mass fraction of the wind contained in zones behind strong shocks must be a property of any radiation-driven wind-shock model. Gas heated to X-ray–emitting temperatures is too highly ionized to have any significant line opacity at wavelengths where photospheric radiation exists in large amounts.

These initial numerical explorations indicate that significant quantities of X-ray–emitting plasmas can be generated in hot star winds by the line-force instability, but very little quantitative comparison between theory and observations has yet occurred. Furthermore, structure on larger scales appears to also exist in hot star winds, as evidenced by blueward-migrating discrete absorption components seen in wind line profiles (Massa et al. 1995). So while the line-force instability mechanism probably leads to some X-ray

[1] University of Wisconsin—Madison, Department of Astronomy, 475 North Charter Street, Madison, WI 53706; cohen@duff.astro.wisc.edu, cassinelli@madraf.astro.wisc.edu.

[2] University of Wisconsin—Madison, Fusion Technology Institute, 1500 Johnson Drive, Madison, WI 53706.

[3] Applied Research Corporation, 8201 Corporate Drive, Suite 1120, Landover, MD 20785; waldron@indy.arclch.com.

emission in OB stars, it cannot account for all the observed time-dependent phenomena, and so other types of wind shocks may be contributing to the X-rays.

There are several types of shock mechanisms that might plausibly occur in OB star winds that could lead to appreciable X-ray emission. In their numerical explorations of the line-force instability, Feldmeier, Puls, & Pauldrach (1997b) have found that a strong perturbation at the base of the wind can cause collisions between dense shells far out in the wind flow. These calculations represent a different mechanism than the basic line-force instability in which a shock-filled wind can be generated from very small perturbations or simply from self-excited noise (Cooper 1994). The shells found by Feldmeier et al. (1997b) are dense and the compression is large, so this phenomenon can lead to large emission measures. The X-ray emission thus generated can exceed that from the instability-generated shocks themselves in the dense winds of O supergiants, but the application of this shell collision model to lower density B star winds is uncertain. Shocks can also form in corotating interaction regions (CIRs) if the wind properties vary over the surface of the star, due perhaps to spots or magnetic field structure (Mullan 1984; Cranmer & Owocki 1996).

If strong forward shocks and magnetic fields are present in stellar winds, then relativistic electrons may be produced via first-order Fermi acceleration. Inverse Compton scattering of photospheric UV radiation off these fast electrons might be able to produce nonthermal hard X-ray emission in O supergiants (Chen & White 1991). Finally, in addition to these various shock mechanisms, low-density stellar winds may be heated by the friction generated when the ion and electron flows become decoupled (Springmann & Pauldrach 1992).

Recent high-energy observations are generally in accord with the wind-shock paradigm. Hillier et al. (1993) show that *ROSAT* observations of ζ Pup (O4 If) have far too much soft X-ray emission for the X-rays to arise in a coronal zone beneath a spherically expanding wind. Higher resolution BBXRT observations of the same star (Corcoran et al. 1993) show evidence of wind attenuation consistent with the X-rays arising at a mean distance of about $3.5R_*$, which is generally in accord with the predictions of wind-shock models. Similar results were obtained for the two O stars δ Ori and λ Ori from *ASCA* observations (Corcoran et al. 1994). Cohen et al. (1996) used both *ROSAT* observations and higher resolution *EUVE* spectroscopy of ϵ CMa (B2 II) to show that the EUV and X-ray emission arises within the stellar wind flow, not at the base of the wind or external to the wind. In that case, individual lines of Fe XV and Fe XVI were directly observed to be attenuated by He^+ to a degree that is consistent with hot plasma more or less evenly distributed throughout the wind beyond a few tenths of a stellar radius. Additionally, the distribution of plasma temperatures derived from the ϵ CMa data is similar to the results of numerical simulations of the line-force instability (Cohen et al. 1996).

The three major predictions of most wind-shock models, and specifically the line-force instability mechanism, that can be tested with the currently available low- and moderate-resolution X-ray telescopes are the degree of wind-attenuation, the plasma temperature distribution, and the shock "filling factor." As mentioned earlier, the mass fraction of the wind that is shock-heated for *any* wind-shock model must be small in order for the wind to retain enough moderately ionized material to continue to absorb photospheric radiation. However, it should be kept in mind that large emission measures can be achieved in high compression shocks with high-density material flowing into them. We define the filling factor as the ratio of the observed X-ray emission measure to the total wind emission measure calculated assuming a smooth, spherically symmetric wind, as we describe in § 4.5.

Besides showing a continuous distribution of temperatures, the line-force instability mechanism generates many more weak shocks than strong shocks because the shock temperature is proportional to the square of the shock velocity, leading to more warm ($T \lesssim 10^6$ K) gas than hot ($T \gtrsim 3 \times 10^6$ K) gas. The line-force instability mechanism rarely leads directly to shocks that produce very hot gas ($T \gtrsim 10^7$ K) because the shock velocities are generally not more than a few hundred km s^{-1} (Cooper 1994). This, in any case, is true when the instability is seeded by small perturbations at the lower boundary. Shell collisions can have very high velocities, however, when large perturbations are assumed at the base of the wind (Feldmeier et al. 1997b).

The low-resolution *ROSAT* PSPC has been used to determine the plasma temperature distribution and shock filling factor of many O and B stars. The plasma temperatures are nearly always below $T \sim 10^7$ K, as the line-driven instability suggests (Hillier et al. 1993; Cohen et al. 1996; Feldmeier et al. 1997a). The filling factors for massive O star winds are less than 1% (Feldmeier et al. 1997a), a result that is also consistent with general wind-shock models. However, the recent survey by Cohen, Cassinelli, & MacFarlane (1997) has shown that the fraction of the wind needed to reproduce the observed X-ray emission measures increases with later spectral subtypes. Unlike O stars, B0 and B1 stars have filling factors of more than 10%. This percentage could be lower if the mass loss rates have been underestimated, but for mid-B stars and some late-B stars, the filling factors are simply too large to be explained by wind shocks (Schmitt et al. 1993; Berghöfer & Schmitt 1994; Cohen et al. 1997). Cohen et al. (1997) speculated that the wind shocks that are probably responsible for the observed X-ray emission of O stars may be augmented by other mechanisms for early B stars and that these other mechanisms completely take over in at least some late-B stars. Indeed, there is growing evidence for high-energy processes in stars that are too cool to have radiation-driven winds and too hot to have classical coronae. The evidence includes strong X-ray emission from young late-B stars (Schmitt et al. 1993), from Herbig Ae/Be stars (Zinnecker & Preibisch 1994), from Bp/Ap stars in the young open cluster NGC 2516 (Dachs & Hummel 1996), and weaker X-ray emission from late A stars (Simon, Drake, & Kim 1995), as well as chromospheric emission from A and early F stars (Walter, Matthews, & Linsky 1995; Freire Ferrero et al. 1995).

So if some early-type stars have high-energy emission that cannot be explained in the context of radiation-driven winds and the line-force instability mechanism, it behooves us to reexamine the applicability of the wind-shock paradigm to the O and very early B stars that are generally considered to provide the best evidence for wind shocks. The B0 V star τ Sco is an ideal candidate for this study because of several unusual properties including its youth (Kilian 1992), pole-on viewing angle (Uesugi & Fukuda

1982; Waters et al. 1993), equatorial wind density concentration (Waters et al. 1993), and anomalously strong wind (Walborn, Parker, & Nichols 1995). Also, τ Sco has the largest X-ray luminosity and hardest spectrum of any of the 27 B stars observed by Cohen et al. (1997). The star's properties will be further discussed in § 2. *ASCA* is currently the best instrument for carrying out such an investigation because of its superior spectral resolution and sensitivity to hard X-rays (which will be discussed in § 3). If the X-ray properties of τ Sco cannot be explained by the line-force instability mechanism alone, it will be a strong piece of evidence that other high-energy mechanisms are in operation in a subset of O and early B stars. By identifying other X-ray–anomalous early-type stars, it may be possible both to explain the X-ray properties of τ Sco itself and to gain insight into the transition from purely wind-related X-ray emission in O stars to purely coronal emission in late-type stars.

The unprecedentedly high spectral resolution of the *ASCA* data also serves several other purposes. In fitting the spectra, we will be testing the limits of the plasma codes and their large compilations of atomic data, which have been used successfully in the past to fit lower resolution X-ray data. We will measure the fluxes in a few individual strong emission-line complexes, verifying the thermal nature of the X-rays and giving us another way to constrain the temperature of the emitting plasma. Finally, the *ASCA* spectrum will serve as a guide to what we can expect from the much higher resolution data to come from the *AXAF* grating spectrometers.

2. THE STAR, τ SCORPII

Some of the properties of the MK standard (Morgan & Keenan 1973) B0 V star τ Sco are listed in Table 1. This star has been the subject of many studies—both theoretical and observational—of photospheres, winds, and X-ray emission. In a sense, it has become a benchmark hot star for studies in these fields, a slightly cooler counterpart to the early O star ζ Pup (O4 If). Like many stars that have become benchmarks, increased scrutiny has shown τ Sco to be unusual in many important ways. Additionally, a recent study has adjusted its spectral subtype slightly (B0.2 V; Walborn et al. 1995).

TABLE 1

STELLAR PARAMETERS FOR τ SCO

Quantity	Value
Spectral Type	B0 V[a]
l, b (deg)	352, 12[b]
m_v	2.82[c]
D (pc)	231[d]
N_H (cm^{-2})	2.7×10^{20}[e]
T_{eff} (K)	31400[c]
log g (cm s^{-2})	4.24[c]
log L_*($L_\odot$)	4.69[d]
V sin i (km s^{-1})	20[f]
$\dot{M}$ ($M_\odot$ yr^{-1})	3.1×10^{-8}[g]
v_∞ (km s^{-1})	2400[g]

[a] Morgan & Keenan 1973, but sometimes classified B0.2 V.
[b] Member of the Sco-Cen OB association.
[c] Kilian 1992.
[d] Calculated using the observed spectral type and visual magnitude and the calibration of Straizys & Kurielene 1981.
[e] Fruscione et al. 1995.
[f] Uesugi & Fukuda 1981.
[g] Theoretical values calculated from the line-force parameters of Abbott 1982 and using the Kudritzki et al. 1989 "cooking formula."

The earliest UV observations showed τ Sco to have relatively strong wind absorption lines (Jenkins, Morton, & York 1974; Rogerson & Upson 1977). Indeed, Walborn et al. (1995) have classified τ Sco as one of several OB stars that have stronger UV wind signatures than other stars of the same spectral subtype and luminosity class. The observations of UV lines include several highly ionized species like N V and O VI, which led Lamers & Rogerson (1978) to deduce a wind temperature of 2×10^5 K. Although X-rays from OB stars had not yet been discovered, Cassinelli & Olson (1979) proposed that the "superionization" observed in OB stars is due to Auger ionization by X-rays. Because τ Sco is a strong X-ray source, it is now generally accepted that X-ray photoionization is responsible for the high mean ionization, and presumably the wind temperature is not especially high (MacFarlane, Cohen, & Wang 1994). The N V and O VI lines, besides being unusually strong, also have strange profiles (Lamers & Rogerson 1978). The absorption troughs extend well longward of line center. These profiles can be interpreted as evidence either for turbulence or for infall with velocities of a few hundred km s^{-1}.

The star has a very low projected rotational velocity of only 20 km s^{-1} (Uesugi & Fukuda 1982). Because early-type stars should have large rotational velocities, this implies that we are viewing τ Sco nearly pole-on. The redshifted absorption in the superionized wind may then be evidence not of wind infall back onto the photosphere but rather of polar wind material streaming toward equatorial regions, perhaps to a disk. Bjorkman & Cassinelli (1993) have shown that rapid rotation can cause wind material to be focused toward the equator and form a disk that may give rise to the Be phenomenon. Indeed, Waters et al. (1993) observed several IR hydrogen Brackett lines in emission in the spectrum of τ Sco. These authors suggest that τ Sco may be a weak, pole-on Be star and Zaal, Waters, & Marlborough (1995) have suggested that such low-mass Be disks may be a relatively common phenomenon. Furthermore, if there is magnetic activity on τ Sco, then the pole-on viewing angle may have implications for our view of the effects of coronal loops, spots, and/or enhanced wind outflow.

Recent detailed high-resolution spectroscopy and atmosphere modeling of B stars in clusters has been carried out by Kilian (1992, 1994). In this work, very precise abundances of important elements were derived (see Table 2), and line strengths and profiles were used to determine T_{eff} and log g. Based on this analysis, the stars in the study were placed on an empirical H-R diagram and compared with isochrones. Of the 25 stars in Kilian's study, this analysis showed τ Sco to be the youngest—being on the main sequence for less than 10^6 yr.

Finally, previous X-ray studies with *Einstein* (Cassinelli 1985; Swank 1985) and *ROSAT* (Cassinelli et al. 1994; Cohen et al. 1997) have shown that the X-ray emission from τ Sco is very strong and unusually hard for its spectral subtype. The *Einstein* SSS data show significant flux up to about 3 keV, although no emission lines could be clearly seen (Cassinelli 1985). A simple two-temperature model fit requires one component with a temperature of about 20×10^6 K, although the properties of this component

TABLE 2

PLASMA ABUNDANCES USED IN SPECTRAL MODELING

Element	Abundance[a]	Abundance[b]
He	−0.78	1.1
C.....	−3.62	0.6
N	−3.91	1.3
O	−3.41	0.5
Ne	−3.85	1.2
Mg.....	−4.34	1.2
Al	−5.64	0.8
Si	−4.43	0.7
S	−4.95	0.7
Fe.....	−4.67	0.5

[a] Abundance by number, expressed logarithmically with respect to hydrogen, taken from Kilian 1994.

[b] Ratio of elemental abundance from Kilian (1994) to solar elemental abundance from Anders & Grevesse 1989.

could not be well constrained (Swank 1985). The *ROSAT* data, while not sensitive to the presence of very hot ($T \gtrsim 10^7$ K) gas, showed that some attenuation of the soft X-rays by partially ionized wind material was probably occurring. Once corrected for this attenuation, the intrinsic X-ray luminosity in the 0.1–2.4 keV bandpass was determined to be 2.2×10^{32} ergs s^{-1}, giving $L_X/L_{\rm Bol} \sim 10^{-6}$ (Cohen et al. 1997). The corresponding emission measure is roughly equal to the full wind emission measure calculated from the *theoretical* mass loss rate. The purpose of this paper is to use higher resolution X-ray data to verify the presence of very hot plasma and to characterize it.

3. THE DATA

The data discussed in this paper were collected on 1994 September 4–5 in a 20 ks net exposure using the SIS detectors aboard *ASCA*. The *Advanced Satellite for Cosmology and Astrophysics* (*ASCA*; initially known as *Astro-D*) was launched by the Japanese Space Agency on 1993 February 20. An overview of the satellite is given in Tanaka, Inoue, & Holt (1994). The instrument consists of four telescopes, two with Solid State Imaging Spectrometers (SIS0 and SIS1) and two with Gas Imaging Spectrometers (GIS2 and GIS3). These are described by Burke et al. (1991) and Ohashi et al. (1991), respectively. Because of their superior spectral resolution, the SIS detectors' data were used exclusively in this study.

The telescope + SIS effective area, while energy dependent, averages a little more than 100 cm^2 near 1.5 keV. The spectral resolution is $E/\Delta E \approx 20$ near this energy. This is an unprecedented spectral resolution for X-ray telescopes, and as such it provides a hint of the high-quality spectra expected from *AXAF*. This level of spectral resolution, while not allowing for the resolving of lines, does allow for the separation of the strongest lines from the "pseudocontinuum" of many weak emission lines, and the generally even weaker free-free and recombination continuum radiation, expected in thermal sources.

The spatial resolution is significantly poorer than that of the *ROSAT* PSPC with FWHM $\gtrsim 1'$. Fortunately, *ROSAT* observations of τ Sco show that there are no other X-ray sources within several arcminutes of the star, so contamination of the *ASCA* data is not a concern.

Before extracting the source and background counts from the SIS0 and SIS1 detectors, we cleaned the data of hot and flickering pixels and excluded sections of the data based on Earth pointing angle and South Atlantic Anomaly criteria. The total accepted exposure times were 20,101 s for SIS0 and 18,012 s for SIS1. We then extracted the source counts from regions encompassing the entire "Maltese Cross" images and calculated an adjustment to the telescope effective area based on the off-axis angle calculated from the source position on each detector. We extracted a sample of the background X-ray spectrum from a blank region of the same chips that contain the source images. For the data analysis, which we carried out using the XSPEC package, we used the 1994 August 9 versions of the detector response matrices. We also binned some of the higher energy counts to ensure at least 10 counts bin^{-1}, which allowed us to use the χ^2 goodness-of-fit statistic.

4. SPECTRAL ANALYSIS

Stellar X-ray data have typically been fit with highly simplified models in the past because of the crudeness of previously available X-ray data. We agree with the philosophy that models should not be more complicated than the data can support; however, we also believe that they should be as realistic as possible given a reasonable number of free model parameters. Because of the superior spectral resolution of *ASCA* as compared with previous instruments, the models that we use to fit the data can be a little more complex than the simple one- and two-temperature collisional equilibrium models that are generally used. We will, however, adopt the same basic assumptions that traditionally hold, namely, that the zones of emitting plasma are in ionization equilibrium and that they are optically thin to their own line radiation (see Raymond & Brickhouse 1996 for a critical assessment of these, and other, approximations).

Recent modeling of higher resolution EUV and X-ray data (Corcoran et al. 1993, 1994; Cohen et al. 1996) and very high signal-to-noise low-resolution X-ray data (Hillier et al. 1993; Feldmeier et al. 1997b) has shown that models with a continuous temperature distribution in the hot plasma and wind attenuation of the X-ray photons produce better agreement with the data from early-type stars. It is also possible that the nonsolar abundances in these stars should be accounted for when fitting higher quality X-ray data. In modeling our *ASCA* SIS observation of τ Sco, we accounted for the temperature distribution of the emitting plasma and for the nonsolar abundances, but we did not account for the wind attenuation. This is because our earlier modeling of the *ROSAT* PSPC data for τ Sco showed that the wind is optically thick to X-rays only for $E \lesssim 0.5$ keV. Thus, there is only a small overlap between the photon energies for which wind attenuation is important and the spectral range of the *ASCA* SISs. Because only a small region of the spectrum would be affected by wind attenuation and because these energies are where *ASCA* suffers from calibration problems (Dotani et al. 1996), we have chosen simply to exclude those channels with mean energies below 0.8 keV from the model fitting. We also have excluded the small number of channels with energies above 10 keV where statistical fluctuations are large and some systematic uncertainty also appears to be present.

In the most general formulation, the (continuous) plasma temperature distribution is described by a differential emis-

sion measure (DEM), $Q(T)$ (cm^{-3} K^{-1}), such that $dEM = Q(T)dT = n_e n_H dV$ (cm^{-3}). The emitted spectrum is then given by $L_\lambda = \int Q(T)\Lambda(T, \lambda)dT$ (ergs s^{-1} Å^{-1}), where the emissivity per unit wavelength is denoted by $\Lambda(T, \lambda)$ (ergs s^{-1} cm^3 Å^{-1}). $Q(T)$ can, in general, be any arbitrary positive function. For the simple case of an isothermal model, $Q(T) = EM_1\,\delta(T - T_1)$. The form of the differential emission measure reflects the effects of both heating and cooling processes in astrophysical plasmas, as well as averaging over multiple, distinct spatial regions, and in practice it is difficult to disentangle these contributions.

In general, emission lines serve as probes of different temperature plasmas, which to the first order reflect the dependence of the dominant ionization stage on temperature. This implies two basic approaches to extracting information from moderate-resolution X-ray spectra: detailed fitting and global fitting. In the detailed fitting process, the strengths of individual lines are measured and compared with each other, in theory, providing precise temperature and also abundance and density information. This technique requires both high signal-to-noise data and good spectral resolution. In the global fitting technique, spectral models are calculated, convolved with the instrumental response matrix, and the entire model spectrum is compared with the data set. The disadvantage of global fitting is that uncertainties in one quantity effectively get propagated throughout the entire spectrum since many lines are being compared at once; although when data quality is not very good and model uncertainties are large, this is a necessary compromise in order to obtain statistically good fits. The advantage of global fitting is that one makes use of all the data including weak lines, continua, and nondetected features.

Because we see only a few strong emission-line complexes that are separated from the nearby pseudocontinuum of weak lines, we concentrate in this paper on global fitting, although we first discuss the three most prominent line complexes in order to identify the strongest emission lines and get an initial indication of the differential emission measure. The physical goals of the spectral analysis are to ascertain the reality of the very high temperature gas that may be present on τ Sco and specifically to place limits on the form of the differential emission measure above $T \approx 10^7$ K.

4.1. *Individual Line Complexes*

One way to constrain the DEM at high temperatures from the *ASCA* SIS data is to measure and model the luminosities of the strongest high-energy line complexes. In collision-dominated plasmas, individual lines tend to be formed over a relatively narrow range of temperatures. The line luminosity from an isothermal plasma can be predicted from $L_{\rm line} = EM(T)\Lambda(T)$. If one assumes that all the line emission comes from plasma at a specific temperature, then this equation can be inverted to obtain a value for $EM(T)$ at that temperature. Because each line is actually formed in plasma with a range of temperatures, the values of $EM(T)$ formed in this way are actually upper limits, but given enough measurements of different lines, the envelope formed by the determinations from each line are often found to reflect the independently determined shape of the quantity $TQ(T)$, or the logarithmic differential emission measure $dEM/d\log T$.

In Figure 1 we show the three most prominent emission features in the SIS spectra near 1.35 keV, 1.90 keV, and 2.45 keV. We measured the luminosities of these three line complexes by fitting a Gaussian to the features and a power law to the nearby smooth pseudocontinuum regions. Because each feature may have contributions from several lines, we could not be sure of the exact central energy of each feature. We therefore allowed the central energy and width, as well as the amplitude of each of the Gaussian models, to be free parameters. The values we derived are listed in Table 3. The Mg XI, Si XIII, and S XV lines are all the primary resonance transitions ($1s2p \rightarrow 1s^2$) of He-like ions.

The feature near 1.35 keV is the most heavily blended of the three features. One of the strongest of the blended lines at that energy is a line of N-like Fe. There are hints of other line complexes near 1.5 keV and 2.1 keV, probably due to Fe^{+22}, Fe^{+23}, Mg^{+11}, Si^{+12}, and Si^{+13}, but these are not distinct enough to fit as independent entities (see Fig. 2). We will see in the following subsection that the global models we fit contain strong emission features at all five of these energies, as well as at the energies of the three He-like reso-

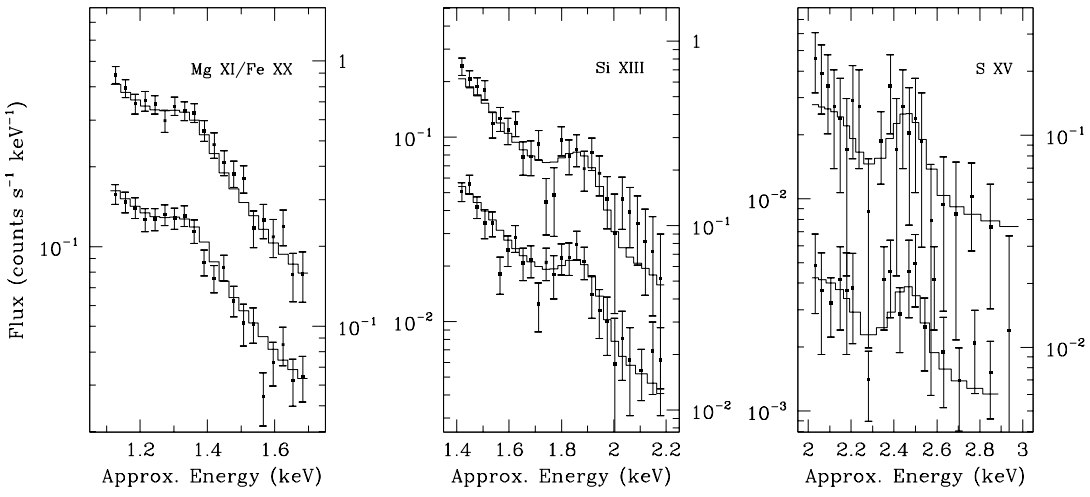

FIG. 1.—We show the best-separated line complexes in both the SIS0 (*top*) and SIS1 (*bottom*) data and the Gaussian fits we made to them in order to derive the line luminosities listed in Table 3. The flux scale on the left refers to the SIS0 data, and the scale on the right refers to SIS1.

TABLE 3

LINE COMPLEX LUMINOSITIES

Central Energy (keV)	Contributing Ions	T_{peak}[a] (MK)	log $(dEM/dT)_{upper}$[b] (cm^{-3} MK^{-1})	Luminosity (ergs s^{-1})	90% Confidence Limit Range (ergs s^{-1})
1.34.....	Mg XI, Fe XX	6.85	54.2	1.27×10^{30}	8.64×10^{29}:2.16×10^{30}
1.88.....	Si XIII	7.00	53.9	1.42×10^{30}	1.03×10^{30}:1.96×10^{30}
2.46.....	S XV	7.15	53.7	6.96×10^{29}	3.13×10^{29}:1.16×10^{30}

[a] Temperature of peak emissivity of the He-like K_α lines according to the Mewe, Gronenschild, & van den Oord 1985 collisional equilibrium code.

[b] Upper limit to the emission measure assuming that the entire contribution to the lines' emissivity is from gas with $T = T_{peak}$.

nance lines. The Mewe, Gronenschild, & van den Oord (1985) collisional equilibrium plasma emissivity table indicates that satellite lines of the He-like lines may contribute a significant fraction of the observable flux in the strongest features we detected. In addition, the weak emission near 3 keV might be due to He-like Ar if there is sufficient very hot plasma. It seems likely that future, higher resolution observations will reveal a spectrum rich in emission features that will be very useful as plasma diagnostics.

The luminosities we derived for each line were used to calculate upper limits to the temperature-dependent differential emission measure, which we list in Table 3. This approximation was derived by computing the $EM(T) = L_{line}/\Lambda(T)$ upper limits and then dividing these values by the characteristic widths of the line contribution function, $\Lambda(T)$, which we took to be half of the temperature of peak emissivity for each line complex. The line strengths indicate that the DEM is decreasing rather strongly with temperature near 10^7 K. This tentative conclusion will be tested in the following subsection using global spectral fitting techniques, although because of the modest resolution of *ASCA*, the complexity of these global models will have to be minimized. Only with future, high-resolution spectroscopic observations in which many lines are unambiguously measured will detailed information about the true shape of the DEM and about the densities in the emitting regions become available.

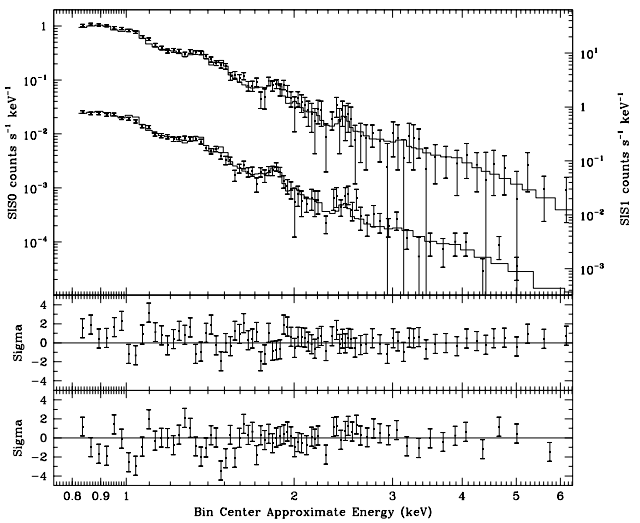

FIG. 2.—In the top panel the SIS0 (*top*) and SIS1 (*bottom*) data are shown with 1 σ statistical uncertainties and the best-fit three-temperature model (*solid lines*). Note that these data and the model are displayed in detector units and that the same model has been fit to both data sets. The bottom two panels show the residuals from the fit to the two data sets with SIS0 in the middle panel and SIS1 in the lower panel.

4.2. *Global Fitting*

The above described analysis of the three line complexes provides evidence of which ions are present in the emitting plasma and gives a first indication of the differential emission measure. In order to make use of all the available data to constrain the DEM, we next performed global fitting. We used the XSPEC package to generate models and simultaneously fit the SIS0 and SIS1 data sets on the photon energy range $0.8 < E(\text{keV}) < 10$. We tried both continuous differential emission measures given by sixth-order Chebyshev polynomials and multitemperature differential emission measures described by the superposition of three different isothermal components. Somewhat surprisingly, the three-temperature models gave significantly better fits than the continuous DEM's. We believe that this is not a true reflection of three separate temperature components but rather is a result of limitations of the Chebyshev polynomial model formulation. In any case, the derived parameter values should be interpreted as a reflection of a continuous differential emission measure.

The three-temperature, optically thin models were computed first from the Raymond & Smith (1977) plasma emission code assuming solar abundances (Anders & Grevesse 1989). No acceptable fit was achieved, so we recomputed these models using the abundances derived from observations of the photosphere of τ Sco (Kilian 1994) which are listed in Table 2. The χ^2 fit statistic was improved in this case, but it was still not consistent with a good fit. We then made models using the Mewe, Kaastra, & Liedahl (1995) plasma code, MeKaL. This is an updated version of the code of Mewe & Kaastra (1994) that contains a more recent version of the ionization balance and new atomic rates for iron L-shell lines. These updated atomic values proved crucial in fitting parts of the spectrum, especially near 1.1 keV, which could not be fit with the Raymond & Smith code. Finally, we refit the data using the MeKaL code but with abundances fixed again at solar values. The fit was unacceptable, indicating that both nonsolar abundances and the updated atomic models in the MeKaL code are necessary to provide a good fit to the data.

To summarize, in order to achieve good fits between model and data we had to exclude data with $E < 0.8$ keV, use the recently updated MeKaL code, use the independently determined elemental abundances, and use at least three different temperature components to approximate the true differential emission measure. Furthermore, because no determination was made of the abundance of nickel by Kilian and nickel is an important contributor of line emission near 1 keV, we allowed the nickel abundance to be a free parameter varying between 0.1 and 10 times the solar value. The fitted values primarily reflect uncertainties in the

TABLE 4

BEST-FIT SPECTRAL MODEL PARAMETERS

Parameter	Best-Fit Value[a]	90% Confidence Range
T_1 (MK)	7.22	7.19:7.45
EM_1 (cm^{-3}).....	3.46×10^{54}	3.16×10^{54}:3.70×10^{54}
T_2 (MK)	12.29	10.19:14.39
EM_2 (cm^{-3}).....	8.11×10^{53}	5.58×10^{53}:1.03×10^{54}
T_3 (MK)	42.6	26.6:>50
EM_3 (cm^{-3}).....	5.91×10^{53}	3.01×10^{53}:9.19×10^{53}

[a] This fit has $\chi^2 = 181.4$ for $\nu = 151$ degrees of freedom, and the interstellar medium column density was allowed to vary on $1.0 \times 10^{20}\ cm^{-2} < N_H < 3.5 \times 10^{20}\ cm^{-2}$.

atomic data for nickel in the MeKaL code and not a truly nonsolar nickel abundance. We stress that all other elements have fixed abundances in our model fitting.

In Table 4 we list the temperatures and emission measures of the three components of the best-fit model. We also list the ranges of these fit parameters corresponding to the 90% confidence limits based on the $\Delta\chi^2$ statistic as described by Lampton, Margon, & Bowyer (1976). In Figure 2 we show the SIS0 and SIS1 data with the best-fit model superimposed. The reduced χ^2 value for this fit is 1.218. Assuming that the statistical uncertainties are accurate, a value this high or higher would be achieved in about 5% of trials in which the model is a correct description of the data. It is likely, however, that in the relatively high signal-to-noise τ Sco data systematic errors are important, and therefore the fit overestimates the χ^2 statistic. Despite this, however, $\chi^2_\nu \approx 1.2$ indicates a much better fit than those found for high signal-to-noise *ROSAT* data (e.g., Hillier et al. 1993). In Figure 3 we show the best-fit, unconvolved model spectrum and the contributions of the three different components to the complete spectrum.

The largest fraction of the total emission measure is in the lowest temperature component. It contributes most of the flux below about 1.2 keV and is probably the dominant contributor to the *ROSAT* data. In order to fit the harder *ASCA* spectrum, two hotter components, in addition to this low temperature component, had to be included. The next highest temperature component has a somewhat smaller emission measure and contributes mostly to the iron-group element L-shell lines a little above 1 keV. The highest temperature component contributes mostly above 2.5 keV, but it also contributes a little to the continuum and emission lines below 2.5 keV. The lines between about 1.5 keV and 2.5 keV, including the strong S XV line complex near 2.45 keV, have contributions from a combination of the three components. The extent of the 90% confidence limits for the parameters T_2, T_3, EM_2, and EM_3 places some constraints on the shape of the true DEM that describes the very hot ($T \gtrsim 10^7$ K) plasma on τ Sco. The emission measure of the hottest component is only a little less than the emission measure of the second component. The hottest component has contributions from plasma over a wider range of temperatures though, so if we use the three-temperature model to approximate a continuous DEM we must conclude that $Q = dEM/dT$ decreases with temperature, but not very steeply. This can also be seen from the $EM(T)$ limits calculated from the individual line fluxes listed in Table 3.

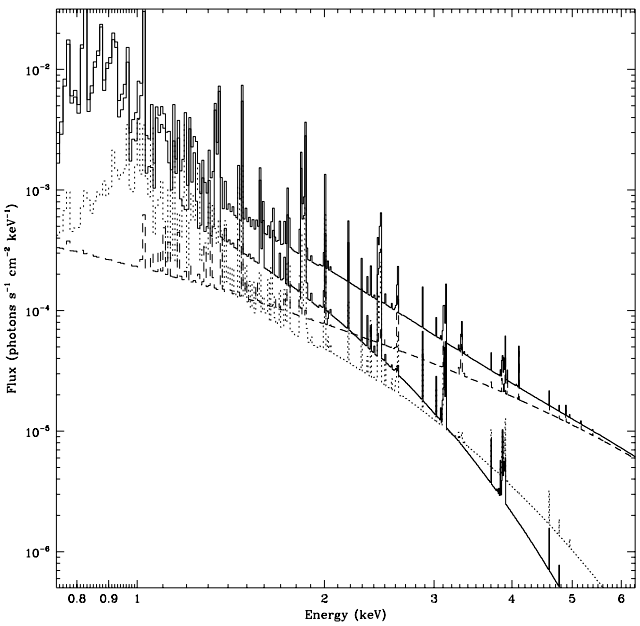

FIG. 3.—We show the best-fit thermal model (*thick solid line*) and the contribution of each of the three temperature components to it: T_1 (*thin solid line*), T_2 (*dotted line*), T_3 (*dashed line*).

In a sense, it is somewhat surprising that we were able to fit the τ Sco *ASCA* spectrum with models not much more complicated than those that traditionally have been used to fit much lower resolution data. Although *ASCA* data may be on the verge of necessitating the rejection of some of the common assumptions, like ionization equilibrium, this data set does not require it. The very high temperatures we find for two of the model components may not reflect true thermal properties of the plasma if ionization equilibrium does not strictly hold.

4.3. *Further Constraints on the Model*

We performed several additional tests of the robustness of the best-fit model described in the previous subsection and especially of the derived properties of the very hot plasma. To further explore the model fitting results and also to examine the effects of selectively altering the line strengths in the plasma codes, we refit the data allowing the nickel abundance of each component to be a completely free parameter. In this case, the best-fit χ^2 value did improve significantly, to $\chi^2_\nu = 1.14$ [corresponding to a probability of $P(\chi^2) \approx 0.15$]. But in order to get this improvement, the nickel abundance for the second component had to be increased to almost 1000 times the solar value. The emission measure of this component then became very small (about a factor of 10 below that found in the original fit). This exercise may be telling us that the atomic data for nickel in the MeKaL plasma code needs improvement. It also provides a lesson in the spectral fitting of moderate resolution X-ray data, namely, that the fitting routine will use whatever free parameters are available to improve the statistics of the fit, regardless of the physical meaningfulness of the values of those parameters. This lesson should make investigators wary of allowing individual elemental abundances to be completely unconstrained free parameters while using highly simplified temperature models in attempting to fit *ASCA* and other low- and moderate-resolution X-ray data.

Next we set out to test the robustness of the high temperature component of our global model fit. First, we refit the data sets with the same three-temperature MeKaL

model on the photon energy interval $0.8 < E(\mathrm{keV}) < 10$, but this time forcing all the temperature components to be at or below 12×10^6 K (12 MK). In this case, the best-fit χ^2 statistic was $\chi^2_\nu = 1.63$. This value is unacceptable, and the fit can be rejected at better than the 99.9% confidence level. We show this model along with the data in Figure 4. This experiment shows that temperature components above $T \approx 12$ MK are required to fit the data above $E_x \approx 1.5$ keV.

We performed a final test to examine whether the hottest model component was required only in order to fit the very low signal-to-noise data above the S XV line complex near 2.5 keV. We refit the data with a three-temperature MeKaL model with the Ni abundance free to vary between 0.1 and 10 times the solar value, but we restricted the data that we fit to $0.8 < E(\mathrm{keV}) < 2.6$. In this case, we produced a best-fit model of a similar quality to our initial fit. Perhaps surprisingly, the model parameters we derived are very similar to those derived for the data set that includes the bins covering the range of photon energies from 2.6 keV to 10 keV. Specifically we still find a hot, third component with a temperature in excess of 20 MK. The lower limit (90% confidence limit) to the emission measure of this very hot component is 2.5×10^{53} cm^{-3} and to the temperature is 22 MK. This implies that *independent* of the weak, high-energy ($E > 2.5$ keV) flux in the *ASCA* SIS spectra, the presence of very hot gas is required to explain the data if a purely thermal model is assumed.

4.4. *A Nonthermal Component*

Because the data above 2.5 keV are noisy, we cannot say with certainty that the high-energy emission is thermal. Obviously, because of the line emission, we must conclude that much of the softer X-ray emission is indeed thermal. Additionally, any nonthermal model we fit must be physically plausible, as its presence will be constrained by only a small fraction of the source photons. As shown by the experiment with the completely free nickel abundance model in § 4.3, a low χ^2 statistic in and of itself is not enough to validate a specific type of model. It is only useful for constraining the parameters of models that have already been determined to be realistic.

In order to say more about the applicability of nonthermal models, we fit a model that has the same multitemperature nature as those described in § 4.2 with the added feature of a power-law component having a low-energy cutoff. This model is meant to approximate the calculations by Chen & White (1991). However, unlike their models in which the inverse Compton power-law component is calculated directly from the observed thermal soft X-rays and a specific shock model, ours is purely empirical. Because of the large emission measure and high temperature of the thermal component, it is not clear what type of shock model, if any, is applicable to τ Sco, so computing the inverse Compton spectral component from first principles is too uncertain in this case.

The three-temperature thermal plus power-law model provides a small improvement in the goodness of fit, having $\chi^2_\nu = 1.18$ for 148 degrees of freedom. The best-fit model parameters and their 90% confidence limit ranges are listed in Table 5, and the best-fit model is shown in Figure 5. Note that a temperature of at least 11.6 MK is still required for the hottest of the thermal components and that its emission measure is at least 9.3×10^{53}.

Figure 5 shows that the power-law component makes a significant contribution down to energies below 2 keV. It is possible that this fit provides a good χ^2 statistic simply because the thermal models underestimate the true continuum level. This deficiency in the standard thermal equilibrium models has been noted in the analysis of other stellar X-ray sources (Schrijver et al. 1995).

For this thermal plus nonthermal model, we allowed the low-energy cutoff of the power-law component to be any value greater than 1.5 keV. Below this value of E_{cut}, the photon flux power-law index was taken to be zero. We fit the slope of the power law and the normalization in addition to E_{cut}. The photon-spectral slope we found is between

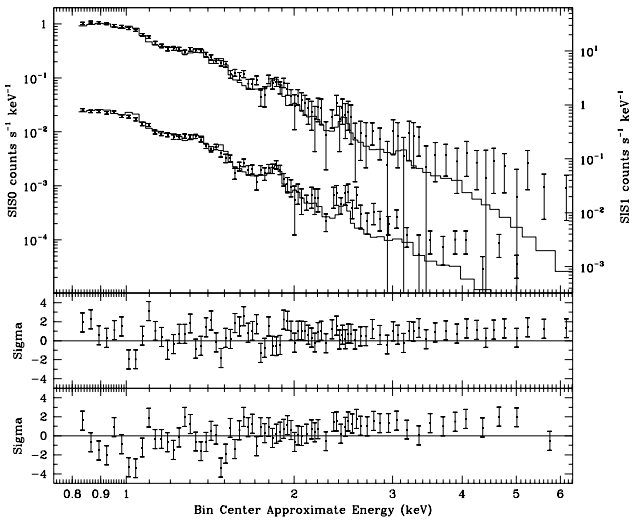

FIG. 4.—The top panel shows the data and best-fit model in which the temperature of each component was forced to be no more than 12 MK. The two lower panels show the residuals from the model fit to the two data sets. Note that at ~1.5 keV and above the model does not adequately fit the data.

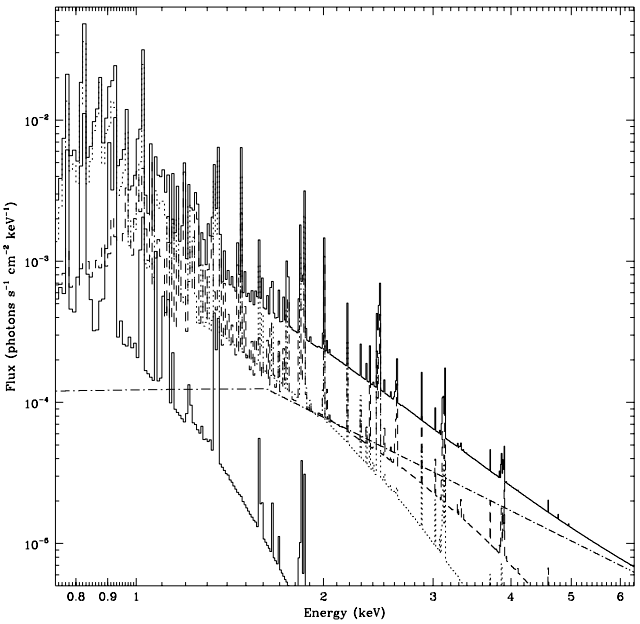

FIG. 5.—We show the best-fit model (*thick solid line*) and the contribution of each of the four components to it: T_1 (*thin solid line*), T_2 (*dotted line*), T_3 (*dashed line*), and nonthermal (*dash-dotted line*).

TABLE 5

BEST-FIT SPECTRAL MODEL PARAMETERS FOR COMBINED THERMAL AND NONTHERMAL MODEL

Parameter	Best-Fit Value[a]	90% Confidence Range
T_1 (MK)	2.56	2.03:3.28
EM_1 (cm^{-3})	2.80×10^{54}	1.11×10^{54}:6.17×10^{54}
T_2 (MK)	7.04	6.60:7.36
EM_2 (cm^{-3})	2.81×10^{54}	2.32×10^{54}:3.20×10^{54}
T_3 (MK)	12.95	11.60:14.33
EM_3 (cm^{-3})	1.20×10^{54}	9.27×10^{53}:1.39×10^{54}
E_{cut} (keV)	1.62	<1.50:2.57
α	−2.20	−2.76:−1.27
F_0 (photons cm^{-2} s^{-1} keV^{-1} at 1 keV)	1.26×10^{-4}	3.86×10^{-5}:2.58×10^{-4}

[a] This fit has $\chi^2 = 174.5$ for $\nu = 148$ degrees of freedom, and the interstellar medium column density was allowed to vary on $1.0 \times 10^{20} cm^{-2} < N_H < 3.5 \times 10^{20} cm^{-2}$.

-2.76 and -1.27, which is consistent with the relationship found by Chen & White (1991) of $j_\nu \propto E^{-(n-1)/2}$ and reasonable values of n, the power-law index of the energy spectrum of relativistic electrons. The normalization of the power-law component is taken as the photon flux density at 1 keV. The value that we find implies that a little more than 10% of the X-ray flux on $0.8 < E(\text{keV}) < 10$ is due to the nonthermal emission mechanism. The relevance of this fit will be discussed in § 5.

4.5. *The Derived Properties of τ Sco*

We can use the best-fit models derived above to calculate the X-ray luminosity of τ Sco. Integrated on $0.8 < E(\text{keV}) < 10$, the thermal model described in Table 4 gives a luminosity, corrected for interstellar extinction, of $L_X = 5.47 \times 10^{31}$ ergs s^{-1}, and $\log L_X/L_{Bol} = -6.53$. This is significantly less than the value of 2.24×10^{32} ergs s^{-1} derived from *ROSAT* PSPC observations over the bandpass $0.1 < E(\text{keV}) < 2.4$. This discrepancy is consistent with our finding that most of the emission measure is due to the lowest temperature component, which radiates mostly below 1 keV. The bulk of the *ROSAT* bandpass X-rays are in the softest bands, below 0.8 keV, and therefore are not included in our *ASCA* data set. The X-ray luminosity above 2.4 keV derived from the *ASCA* data is 6.34×10^{30} ergs s^{-1}. Finally, the X-ray luminosity of the portion of the spectrum above 3.0 keV is a modest, but significant, 4.40×10^{30} ergs s^{-1}. It should be noted that this is comparable to the X-ray luminosity above 100 eV (the entire *ROSAT* bandpass) of normal early B stars (Cohen et al. 1997). These results are basically unchanged if we consider the hybrid thermal plus nonthermal model rather than the purely thermal model. The largest source of error in the quoted luminosities comes from the uncertain distance to τ Sco, and not from statistical errors in the data or uncertainties in the models.

We can use the derived values of the emission measure to determine the "filling factor," which we have defined previously (Cohen et al. 1997) to be the fraction of the available wind emission measure that is being used to produce X-rays:

$$ff = \frac{EM_X}{EM_{wind}} = EM_X \Big/ \int_{R_0}^{\infty} \frac{\dot{M}^2}{[\mu m_H v(r) r]^2 4\pi} dr \ .$$

This quantity is necessarily an approximation because R_0, the radius beyond which strong wind shocks may occur, is somewhat uncertain. We adopt $R_0 = 1.5R_*$ as the point above which wind material may contribute to the production of wind-shock X-rays and use the values of $\dot{M}$ and v_∞ listed in Table 1. We note that a filling factor of unity is not a strict upper limit, since clumping in the postshock regions will increase the emission measure as density squared. However, material accelerated into shocks due to the line-driven instability tends to be rarefied, making it more difficult to achieve large emission measures and filling factors in practice.

We find that the entire wind emission measure for τ Sco is 1.16×10^{55} cm^{-3}. This leads to a total X-ray filling factor of 0.42 and a combined filling factor for only the two hotter temperature components of 0.12. For the hybrid thermal plus nonthermal model, the hottest thermal component accounts for an emission measure filling factor of 0.09. The *ROSAT*-derived emission measure filling factor is 1.8 (Cohen et al. 1997). These values are to be contrasted with the results of the line-force instability shock simulations for B stars in which the filling factors are typically $\lesssim 0.01$ (Cooper 1994; Cohen et al. 1996).

All the model-fitting experiments described above reinforce the robust result that there is a significant quantity of very fast electrons present on τ Sco. If the observed X-rays are purely thermal, then these fast electrons must be produced in regions having temperatures in excess of 25 MK. If they are nonthermal, then there is a power-law component of the spectrum with a slope of about -2 and a luminosity in excess of 10^{31} ergs s^{-1}. Even in the case of a nonthermal source, there still is evidence for a large quantity of thermal emission from plasma with temperatures in excess of 12 MK.

For the thermal model, we can say specifically that the 90% confidence limits on the fitted parameters indicate that the emission measure of gas with temperatures at least as high as 12 MK is more than $\frac{1}{7}$ of the total X-ray emission measure. Furthermore, the confidence limits on the parameters describing the hottest component indicate the presence of a smaller, but still significant, quantity of very hot plasma with temperatures of several tens of megakelvins. In the next section, we will discuss these results in terms of what is known about shocks in radiation driven winds and about the peculiar properties of τ Sco itself. We will also evaluate the relevance of the nonthermal model.

5. DISCUSSION

We now have the information necessary to evaluate the application of the wind-shock picture of X-ray emission to τ Sco. We begin by assessing the implications of the power-law model, and then we compare the two major results we

have derived, the quantity of hot plasma and its temperature distribution, with the commonly accepted line-force instability mechanism for producing wind shocks. We also consider other wind-shock models and finally nonwind mechanisms for producing hard X-ray emission.

The inverse Compton process that could lead to the nonthermal power-law spectral component discussed in § 4.4 has been explored theoretically, but it has never been directly observed. The crucial ingredient of this model is the presence of large quantities of relativistic electrons. The fast electron production mechanism is first-order Fermi acceleration, and the synchrotron emission requires magnetic fields of a few gauss extending into the wind where the shocks occur. The shocks themselves must be strong, with large compression in order to produce enough relativistic electrons to account for the large nonthermal component. The simulations of this process have been performed for stars with winds much more dense than that of τ Sco (Chen & White 1991). It is not clear if shocks in low-density winds can accelerate an appreciable number of electrons to relativistic velocities.

The electrons that eventually are accelerated to relativistic velocities originate in the high-energy tail of the velocity distribution in the shock-heated plasma. So the ratio of nonthermal to thermal X-ray flux is an indication of the efficiency of the particle acceleration mechanism. For τ Sco we find that a very high efficiency is required to get a good fit to the data. According to our model fitting, more than 1/10 of the shock energy must be converted to nonthermal emission, which is greater than the maximum value considered to be reasonable by Chen & White (1991). Furthermore, these authors describe how the relativistic electrons, when present in large quantities, can modify the shock structure, among other things weakening shocks so that lower postshock temperatures are generated. Strong nonthermal emission thus has the effect of suppressing hot thermal shock emission. However, our empirical inverse Compton model fit indicates the presence of a large quantity of hot (temperatures up to 12–14 MK) plasma. For these reasons, we consider the shock-related inverse Compton model to be a very unlikely explanation for the hard X-rays seen in the *ASCA* spectra of τ Sco.

As discussed in the introduction, recent one-dimensional simulations of the line-force instability show a highly structured wind with many shocks (Cooper 1994; Feldmeier 1995). The shocks are, however, relatively weak reverse shocks in which rarefied upstream gas is accelerated into the shock zones. Even the postshock cooling zones do not have very high densities. This structure results in filling factors of 1% or less and usually, but not always, to only a handful of shocks with velocities in excess of 100 km s^{-1}. Stronger and harder emission can be produced by wind shocks if there is a strong perturbation at the base of the wind. But even allowing for such boundary conditions, the filling factors we derived in the last section are at least 10 times more than the values found in the simulations of O supergiants. This filling factor discrepancy could be made less severe if the true mass loss rate of τ Sco were actually larger than the application of standard line-driven wind theory predicts (Abbott 1982; Kudritzki et al. 1989). Indeed, Walborn et al. (1995) claim that τ Sco has a stronger wind than other stars of its spectral subtype. Additionally, Cohen et al. (1997) have shown that wind-shock filling factors increase as one considers later B spectral subtypes, and they suggest that the mass loss rates of these stars might be systematically underestimated.

The X-ray temperatures we find from the *ASCA* observations of τ Sco of $T \gtrsim 25$ MK are greater than those found in most O stars or any other B stars. Temperatures of shocked gas are of course directly related to the shock strength. An adiabatic shock or the immediate postshock region in general, has a temperature given by $T_s = 1.44 \times 10^5 (v_s/100 \text{ km s}^{-1})^2$ K, where v_s is the velocity of the upstream flow with respect to the shock front (Krolik & Raymond 1985). In order to generate a shock temperature of 12 MK (the minimum temperature required to fit the data even in the presence of a strong power-law spectral component), the shock velocity must be 910 km s^{-1}. The simulations show that shocks generally form in regions of the wind where the flow velocity has already reached an appreciable fraction of the terminal speed. It is very difficult for radiation pressure to further accelerate dense wind streams by nearly 1000 km s^{-1} or more (Cranmer & Owocki 1996). Such large shock velocities involving high-density streams would be required to produce the plasma described by the second temperature component (10–14 MK) in our best-fit thermal model. Generating the plasma described by the third component ($T \gtrsim 25$ MK) via a shock would require a shock velocity of $v_s = 1400$ km s^{-1}. This is a velocity comparable to the maximum blue edge velocity observed in the wind-broadened UV lines of τ Sco (Hamman 1981) and approaches the theoretical terminal velocity of a little over 2000 km s^{-1}. In other words, to produce the very hot gas detailed in § 4 via wind shocks would require taking a significant fraction of the wind at nearly its terminal velocity and running it into a massive, stationary object.

It has, however, been shown recently that large perturbations at the base of a line-driven wind of an O supergiant can cause dense, slow-moving shells to form far out in the flow. Low-density material traveling at approximately the wind terminal velocity can get accelerated into these dense shells producing shock velocities in excess of 1000 km s^{-1}, with an appreciable amount of material getting heated to X-ray emitting temperatures (Feldmeier et al. 1997b). The application of these results to τ Sco is highly uncertain, however, because this star's mass loss rate is about 100 times lower than that of ζ Ori, the star modeled by Feldmeier et al. (1997b), and because the large photospheric perturbations needed to seed such large wind instabilities are ad hoc. Even so, the emission measure filling factors calculated for O supergiants are far below those we find here for τ Sco (Feldmeier et al. 1997b). Therefore, if the line-force instability is to explain the X-ray emission from τ Sco, it must be seeded by very large perturbations, and it must be even more efficient in the relatively low density wind of τ Sco than it is in the massive winds of O supergiants. Further study and modeling of τ Sco is warranted in order to push the line-force instability model to its extremes.

Thus, it seems that the line-force instability mechanism growing naturally from small perturbations as explored in one-dimensional numerical simulations cannot directly account for all of the observed X-rays in τ Sco. This is not to say that the mechanism is not operating. Indeed, it could very well be responsible for the much of the softer X-ray emission, especially if the mass loss rate of the star has been underestimated. The hot gas, with temperatures in excess of

10 MK, is most likely produced by some other mechanism, however. This alternate mechanism could conceivably involve wind shocks of a different type.

MacFarlane & Cassinelli (1989) have shown that such conditions can be produced by a driven-wave shock propagating through a stellar wind. In fact, τ Sco was used as a test of their model in the original study. By manipulating the velocity jump across the shock front via the interaction of a fast wind stream with a slow one, these authors were able to produce very large shock temperatures and a high degree of compression in the postshock cooling zone, leading to the requisite large emission measures. The difficulty with this model, like the difficulty with the line-force instability model with large seed perturbations, is the ad hoc nature of the driving of the shock. There is no observational evidence for such large changes in the bulk wind velocity structure of τ Sco in either the optical, UV, or the X-ray.

Another potential source of fast wind interactions would be related to the possibility of wind infall, as seen in the O VI and N V lines (Lamers & Rogerson 1978; Howk, Cassinelli, & Lamers 1997). If material is falling back through the wind toward the photosphere at several hundred km s^{-1} then collisions with outflowing material at slightly larger velocities could lead to the very high temperatures we observe. The status of τ Sco as a Brackett emission star (Waters et al. 1993) could be related to infall according to the wind-compressed disk model (Owocki, Cranmer, & Blondin 1994) or the presence of high-density quasi-stationary material sometimes seen above the photospheres of Be stars (Smith et al. 1997). In all these scenarios dense, nearly stationary material might be in a position to interact with a much faster, rarefied wind component.

Finally, we may ask whether a magnetically confined corona could be responsible for the hard X-ray emission detected with *ASCA*. The quantity of hot gas could easily be accounted for by a corona if we crudely apply the scaling associated with the limits on the maximum amount of coronal X-ray emission in late-type dwarfs. Haisch & Schmitt (1996) claim that surface saturation of the coronal dynamo in G through M dwarfs is reached when $L_X \approx 10^{-3} L_{\rm Bol}$. Even allowing for a large uncertainty in the application of this limit to purported coronae on hot stars, the X-ray luminosity we derived for τ Sco is several orders of magnitude below this saturation limit. The high temperatures we derive for the plasma on τ Sco are hotter than the typical quiescent coronal emission of late-type stars but are comparable to that found in the most active coronal sources (Schmitt et al. 1990; Haisch & Schmitt 1996). The observed soft X-rays would probably suffer a lot of attenuation due to the stellar wind, and a significant quantity of soft X-rays are seen in the *ROSAT* observation of τ Sco (Cohen et al. 1997). The actual extent of wind attenuation of the X-rays has not been studied quantitatively, however, and it may be possible to reconcile it with a coronal origin if the mass loss rate is relatively low, or if the mass-loss is patchy, as it is on the Sun, where it is mostly concentrated in coronal holes.

So the observed properties of τ Sco are not necessarily inconsistent with the presence of an X-ray–emitting corona, but is there any reason to believe that τ Sco can support such a magnetic structure? Several of its peculiar properties may actually provide support for the coronal hypothesis. Be stars, which τ Sco may be (Waters et al. 1993), have occasionally shown evidence for phenomena that may be related to surface magnetic fields. These include the confinement of a quasi-stationary slab suspended above the photosphere (Smith et al. 1997) and a giant hard X-ray flare observed on the classical Be star λ Eri (Smith et al. 1993). Its extreme youth (Kilian 1992) may mean that the remnant of the magnetic field of the natal cloud out of which τ Sco was formed could still be present on the star. This connection between extreme youth and magnetic fields in non–surface-convective stars has been suggested by Schmitt et al. (1993) to explain the observed X-ray emission in very young late B stars.

Recently, Tout & Pringle (1995) have suggested a mechanism by which such a remnant magnetic field could be sustained by a dynamo that taps differential rotation rather than surface convection. The model of a differential rotation driven dynamo producing coronal X-ray emission has also been applied to Herbig Ae/Be stars (Zinnecker & Preibisch 1994). The supposition of differential rotation in this model is ad hoc, but it is not contradicted by any observations. In fact, observations do indicate some sort of bulk motions on the surface of τ Sco (Smith & Karp 1978). These authors detect extra absorption in the blue wings of several photospheric lines. They claim that subsurface convection due to a He^+ ionization zone may actually be occurring. In any case, it is clear from their data that some form of mechanical energy is present in large quantities in the photosphere of τ Sco.

It is also possible that the presence of magnetic fields in conjunction with a radiation driven wind could lead to very strong X-ray emission even without a mechanically heated corona. Babel & Montmerle (1997) have recently proposed such a model to explain the large X-ray flux from the magnetic A0 star IQ Aur. In this model radiation driven wind streams are accelerated up from the two footpoints of a large coronal loop. The two streams, confined by the loop, collide at the top with a shock velocity of nearly twice the flow velocity of each stream.

6. CONCLUSIONS

The X-ray observations of τ Sco indicate that there are unusual high-energy processes occurring on this B0 V star. If shocks are the cause of the X-rays, then the wind shocks in τ Sco must be of extraordinary strength. Either these must directly heat material to $T \gtrsim 25$ MK, or they must be laced with magnetic fields and be strong enough to accelerate electrons to relativistic velocities while also maintaining a large quantity of plasma with temperatures in excess of 12 MK. Either circumstance would severely tax current pictures of wind-shock dynamics. Additionally, no other main sequence single OB star is confirmed to have such hot gas or to have nonthermal X-ray emission. However, nonwind, coronal mechanisms would be just as unprecedented.

The evidence that we have presented in this paper indicates that τ Sco is an unusual B star as far as X-ray properties are concerned, in addition to its other peculiarities, which include pole-on orientation, a possible equatorial disk, extreme youth, an anomalously strong wind, and unusual wind velocity structure. It is unclear which of these properties, if any, are related to its X-ray activity. However, if further evidence in favor of a corona or a hybrid wind-magnetic mechanism is obtained, then it is likely that the star's youth plays some role. τ Sco may be the best studied B star with anomalous X-ray properties, but it by no means

is the only one. The late B stars discovered with *ROSAT* by Schmitt et al. (1993) and Berghöfer & Schmitt (1994) may fall into the same category. In addition, the 5%–10% of B stars detected in the *Einstein* All-Sky Survey (Grillo et al. 1992) and in the *ROSAT* All-Sky Survey (Meurs et al. 1992; Berghöfer et al. 1997) also seem to require non–wind-shock mechanisms to explain their large observed emission measures. It may be, then, that τ Sco is the prototype of a class of anomalously strong and hard X-ray sources among the B stars. As such, further observations could be used to answer some outstanding questions. These observations include higher resolution and higher signal-to-noise X-ray spectroscopy to address the nature of the spectrum above 2.5 keV and detailed investigations of the unusual UV wind-line profiles to see if the infall-shock explanation for the hard X-rays is viable. Additionally, a study of a larger sample of such "τ Sco–type" X-ray B stars might reveal whether youth, nonmonotonic wind velocity fields, projected rotation velocity, or some other unusual property is crucial for the production of anomalously strong and hard X-rays.

Future higher resolution, high-throughput X-ray spectroscopy should shed light on these issues. The separation and measurement of the intensities of more emission lines will allow for a much more precise determination of the temperature distribution of hot plasma on τ Sco. Specifically, if the weak emission near 3 keV can be shown to be thermal, it would rule out a significant inverse Compton continuum. It would also provide even stronger evidence for very hot plasma.

We would like to thank Peter Hofner, Craig Markwardt, and Koji Mukai and the staff of the *ASCA* Guest Observer Facility for advice about the *ASCA* data reduction and analysis. We would also like thank Joe MacFarlane and the referee, Stan Owocki, for several useful suggestions. This research has made use of the SIMBAD database, operated at CDS, Strasbourg, France. It was supported by NASA grant NAG 5-2705 to the University of Wisconsin. W. L. W. was supported in part by NASA contract S-44649-Z.

REFERENCES

Abbott, D. C. 1982, ApJ, 259, 282
Abbott, M. J., & Friend, D. B. 1989, ApJ, 345, 505
Anders, E., & Grevesse, N. 1989, Geochim. Cosmochim. Acta, 53, 197
Babel, J., & Montmerle, T. 1997, A&A, 323, 121
Berghöfer, T. W., & Schmitt, J. H. M. M. 1994, A&A, 292, 5
Berghöfer, T. W., Schmitt, J. H. M. M., Danner, R., & Cassinelli, J. P. 1997, 322, 167
Bjorkman, J. E., & Cassinelli, J. P. 1993, ApJ, 409, 429
Burke, B. E., Mountain, R. W., Harrison, D. C., Bautz, M. W., Doty, J. P., Ricker, G. R., & Daniels, P. J. 1991, IEEE Trans., ED-38, 1069
Cassinelli, J. P. 1985, in The Origin of Nonradiative Heating/Momentum in Hot Stars, ed. A. B. Underhill & A. G. Michalitsianos (NASA Conf. Publ. 2358; Washington: NASA), 2
Cassinelli, J. P., Cohen, D. H., MacFarlane, J. J., Sanders, W. T., & Welsh, B. Y. 1994, ApJ, 421, 705
Cassinelli, J. P., & Olson, G. L. 1979, ApJ, 229, 304
Chen, W., & White, R. L. 1991, ApJ, 366, 512
Cohen, D. H., Cassinelli, J. P., & MacFarlane, J. J. 1997, ApJ, in press
Cohen, D. H., Cooper, R. G., MacFarlane, J. J., Owocki, S. P., Cassinelli, J. P., & Wang, P. 1996, ApJ, 460, 506
Cooper, R. G. 1994, PhD. thesis, Univ. Delaware
Corcoran, M. F., et al. 1993, ApJ, 412, 792
———. 1994, ApJ, 436, L95
Cranmer, S. R., & Owocki, S. P. 1996, ApJ, 462, 469
Dachs, J., & Hummel, W. 1996, A&A, 312, 818
Dotani, T., et al. 1996, *ASCA* News, 4, 3
Feldmeier, A. 1995, A&A, 299, 523
Feldmeier, A., Kudritzki, R. P., Palsa, R., Pauldrach, A. W. A., & Puls, J. 1997a, A&A, 320, 899
Feldmeier, A., Puls, J., & Pauldrach, A. W. A. 1997b, A&A, 322, 878
Freire Ferrero, R., Gouttebroze, P., Catalano, S., Marilli, E., Bruhweiler, F., Kondo, Y., van der Hucht, K., & Talaver, A. 1995, ApJ, 439, 1011
Fruscione, A., Hawkins, I., Jelinsky, P., & Wiercigroch, A. 1994, ApJS, 94, 127
Grillo, F., Sciortino, S., Micela, G., Vaiana, G. S., & Harnden, F. R. 1992, ApJS, 81, 795
Haisch, B., & Schmitt, J. H. M. M. 1996, PASP, 108, 113
Hamman, W.-R. 1981, A&A, 100, 169
Hillier, D. J., Kudritzki, R. P., Pauldrach, A. W. A., Baade, D., Cassinelli, J. P., Puls, J., & Schmitt, J. H. M. M. 1993, A&A, 276, 117
Howk, C., Cassinelli, J. P., & Lamers, H. J. G. L. M. 1997, in preparation
Jenkins, E. B., Morton, D. C., & York, D. G. 1974, ApJ, 194, 77
Kilian, J. 1992, A&A, 262, 171
———. 1994, A&A, 282, 867
Krolik, J. H., & Raymond, J. C. 1985, ApJ, 298, 660
Kudritkzi, R. P., Pauldrach, A., Puls, J., & Abbott, D. C. 1989, A&A, 219, 205
Lamers, H. J. G. L. M., & Rogerson, J. B. 1978, A&A, 66, 417
Lampton, M., Margon, B., & Bowyer, S. 1976, ApJ, 208, 177
Lucy, L. B. 1982, ApJ, 255, 286
Lucy, L. B., & White, R. L. 1980, ApJ, 241, 300
MacFarlane, J. J., & Cassinelli, J. P. 1989, ApJ, 347, 1090
MacFarlane, J. J., Cohen, D. H., & Wang, P. 1994, ApJ, 437, 351
Massa, D., et al. 1995, ApJ, 452, L53
Meurs, E. J. A., et al. 1992, A&A, 265, L41
Mewe, R., Gronenschild, E. H. B. M., & van den Oord, G. H. J. 1985, A&AS, 62, 197
Mewe, R., & Kaastra, J. S. 1994, European Astron. Soc. Newsletter, 8, 3
Mewe, R., Kaastra, J. S., & Liedahl, D. A. 1995, Legacy, 6, 16
Morgan, W. W., & Keenan, P. C. 1973, AR&A, 11, 29
Mullan, D. J. 1984, ApJ, 283, 303
Ohashi, T., Makishima, K., Ishida, M., Tsuru, M., Mihara, T., & Kohmura, Y. 1991, in EUV, X-Ray, and Gamma-Ray Instrumentation for Astronomy II, ed. O. H. W. Siegmund & R. E. Rothschild, Proc. SPIE, 1549, 9
Owocki, S. P., Cranmer, S., & Blondin, J. M. 1994, ApJ, 424, 887
Porter, J., & Drew, J. E. 1995, A&A, 296, 761
Raymond, J. C., & Brickhouse, N. S. 1996, Ap&SS, 237, 321
Raymond, J. C., & Smith B. 1977, ApJS, 35, 419
Rogerson, J. B., & Upson, W. L. 1977, ApJS, 35, 37
Schmitt, J. H. M. M., Collura, A., Sciortino, S., Vaiana, G. S., Harnden, F. R., & Rosner, R. 1990, ApJ, 365, 704
Schmitt, J. H. M. M., Zinnecker, H., Cruddace, R., & Harnden, F. R. 1993, ApJ, 402, L13
Schrijver, C. J., Mewe, R., Van den Oord, G. H. J., & Kaastra, J. S. 1995, A&A, 302, 438
Simon, T., Drake, S. A., & Kim, P. D. 1995, PASP, 107, 1034
Smith, M., Cohen, D., Hubeny, I., Plett, K., Basri, G., Johns-Krull, C. M., MacFarlane, J. J., & Hirata, R. 1997, ApJ, 481, 467
Smith, M. A., Grady, C. A., Peters, G. J., & Feigelson, E. D. 1993, ApJ, 409, L49
Smith, M. A., & Karp, A. H. 1978, ApJ, 219, 522
Springmann, U. W. E., & Pauldrach, A. W. A. 1992, A&A, 262, 515
Straizys, V., & Kuriliene, G. 1981, Ap&SS, 80, 353
Swank, J. H. 1985, in The Origin of Nonradiative Heating/Momentum in Hot Stars, ed. A. B. Underhill & A. G. Michalitsianos (NASA Conf. Publ. 2358; Washington: NASA), 86
Tanaka, Y., Inoue, H., & Holt, S. S. 1994, PASJ, 46, L37
Tout, C. A., & Pringle, J. E. 1995, MNRAS, 272, 528
Uesugi, A., & Fukuda, I. 1982, Revised Catalog of Stellar Rotational Velocities (Kyoto: Kyoto Univ.)
Walborn, N. R., Parker, J. W., & Nichols, J. S. 1995, International Ultraviolet Explorer Atlas of B-Type Spectra from 1200 to 1900 E (NASA Ref. Publ. 1363; Washington: NASA)
Waldron, W. L. 1984, ApJ, 282, 256
Walter, F. M., Matthews, L. D., & Linsky, J. L. 1995, ApJ, 447, 353
Waters, L. B. F. M., Marlborough, J. M., Geballe, T. R., Oosterbroek, T., & Zaal, P. 1993, A&A, 272, 9
Zaal, P., Waters, L. B. F. M., & Marlborough, J. M. 1995, A&A, 299, 574
Zinnecker, H., & Preibisch, T. 1994, A&A, 292, 152